Energy Detector based Time of Arrival Estimation using a Neural Network with Millimeter Wave Signals

Xiaolin Liang[1], Hao Zhang[1, 2] and T. Aaron Gulliver[2]
[1] College of Information Science and Engineering, Ocean University of China
Qingdao 266100 – China
[e-mail:xiaolin87liang@163.com]
[2] Department of Electrical Computer Engineering, University of Victoria
Victoria V8P 5C2 – Canada
[e-mail: zhanghao@ouc.edu.cn, agullive@ece.uvic.ca]
*Corresponding author: Hao Zhang

Received March 8, 2015; revised March 1, 2016; revised April 6, 2016; accepted April 15, 2016; published July 31, 2016

Abstract

Neural networks (NNs) are extensively used in applications requiring signal classification and regression analysis. In this paper, a NN based threshold selection algorithm for 60 GHz millimeter wave (MMW) time of arrival (TOA) estimation using an energy detector (ED) is proposed which is based on the skewness, kurtosis, and curl of the received energy block values. The best normalized threshold for a given signal-to-noise ratio (SNR) is determined, and the influence of the integration period and channel on the performance is investigated. Results are presented which show that the proposed NN based algorithm provides superior precision and better robustness than other ED based algorithms over a wide range of SNR values. Further, it is independent of the integration period and channel model.

Keywords: energy detector, millimeter wave, time of arrival

This research was supported by the Nature Science Foundation of China under Grant No. 60902005, the Nature Science Foundation of China under Grant No. 41527901, and the International Science and Technology Cooperation Projects of Qingdao under Grant No. 12-1-4-137-hz.

http://dx.doi.org/10.3837/tiis.2016.07.010 **ISSN : 1976-7277**

1. Introduction

The rapid developments and increasing demands of wireless telecommunication systems have motivated research from both academia and industry on 60 GHz millimeter wave (MMW) technology. These signals are well suited for many applications such as high definition television (HDTV) and 8 K digital cameras. The advantages include several GHz of unlicensed spectrum [1], precise time and multipath resolution [2], and robustness to interference [3][4]. As a consequence, 60 GHz MMW technology is preferred for future gigabit wireless networks [5][6] such as wireless body area networks [7], and this has motivated significant research on the 60 GHz frequency band [8]. This technology has tremendous potential for precise time of arrival (TOA) and range estimation applications, as current solutions based on ultra-wide band (UWB) signals provide poor performance. However, TOA estimation is still challenging because of complex signal environments due to multipath fading and interference.

Many TOA estimation algorithms have been developed [9][10][11][12][13]. The majority of these algorithms employ either a coherent receiver such as a matched filter (MF), or a non-coherent receiver such as an energy detector (ED). A MF can provide excellent TOA estimation even in multipath environments. However, it requires accurate channel estimation, correlator synchronization, and a high sampling rate, so complexity is an issue. Thus, a MF is not practical in many applications, particularly when 60 GHz MMW signals are employed [14]. Conversely, an ED does not require accurate channel estimation and synchronization as only the signal energy is used. Further, a low sampling rate can be employed which reduces the complexity. Thus, an ED is employed here for TOA estimation. An ED consists of four components: a band-pass filter (BPF), a squaring operator, an integrator, and a decision device [14]. The integrator output is compared with a threshold, and the first energy block exceeding the threshold is used as the TOA estimation.

The main challenge with TOA estimation using an ED is the choice of a suitable threshold. Many ED based threshold selection algorithms have been developed. A threshold selection algorithm for TOA estimation based on the skewness of the energy block values was proposed in [9]. In [10], a normalized threshold based on the kurtosis of these values was introduced. A normalized threshold based on the ratio of the minimum and maximum block energies was proposed in [11]. In [12], an algorithm for threshold selection was presented which is based on the skewness and maximum slope of the energy block values. However, there are several problems with these approaches. First, it is difficult to estimate the signal-to-noise ratio (SNR), which makes threshold determination challenging. Second, the resulting performance can be very poor when the SNR is low, i.e. less than 10 dB. Further, the integration period has a significant effect on performance, and the best period is typically a function of the SNR. In addition, the best algorithm given in [12] is applicable only to UWB systems, and may not provide acceptable performance in other systems. Thus obtaining accurate TOA estimates using an ED is problematic

Neural networks (NNs) have been widely employed in statistical signal processing applications [15]. To improve the accuracy, the weights in different layers can be adapted automatically. Further, artificial neural networks (ANNs) can provide robust nonlinear approximations to complex relationships through self-learning and self-adaptation. Consequently, it is a very flexible mechanism for characterizing the relationship between inputs and outputs according to the training data.

Given the difficulties inherent in existing ED based TOA estimation algorithms, a 60 GHz NN based TOA estimation algorithm is introduced which employs the kurtosis, skewness, and curl of the energy block values. Regression problems can be solved using a back-propagation neural network (BPNN). Results are presented which show that the proposed NN based algorithm provides superior precision and better robustness for TOA estimation using 60 GHz MMW signals than other techniques over a wide range of SNR values, especially low SNRs.

The remainder of this paper is organized as follows. The system model is presented in the next section. Section 3 considers the statistical characteristics of the received energy block values. A NN based threshold selection algorithm for TOA estimation is introduced in Section 4, and some performance results are given in Section 5. Finally, some conclusions are provided in Section 6.

2. System Model

Typically, on-off keying, pulse amplitude modulation, or pulse position modulation (PPM) is used in UWB systems [16]. PPM is widely employed in multiple access and high-speed wireless communication systems [17] [18], as it is robust to interference [19] and has good spectral efficiency [20]. Several statistical channel models have been developed for 60 GHz signals such as those in the IEEE 802.15.3c and ECMA 387 standards. The IEEE 802.15.3c standard [21] was developed to support the transmission of data within a few meters at a minimum data rate of 2 Gbps. Both line of sight (LOS) and non-line of sight (NLOS) channel models are provided for indoor residential, indoor office, industrial, outdoor, and open outdoor environments [22][23].

Several *M*-ary PPM signal waveforms have been proposed for 60 GHz MMW systems [24]. In this paper, the 60 GHz PPM signal is given by

$$f(t)=\sum_{y=-\infty}^{\infty} x\left(t-yT_s-B_yT_c-a_y\varepsilon\right) \tag{1}$$

where y and T_s are the frame index and frame duration, respectively. The time-hopping codes are $B_y \in (0,1,....,N_h-1)$, where $N_h=T_s/T_c$ is the number of possible chip positions in a frame, and the chip duration is T_c. ε is the PPM time shift employed when a_y=1, and there is no time shift when $a_y=0$. The pulse waveform is

$$x(t)=\frac{\sqrt{2}}{\alpha}\exp\left(-2\pi\frac{t^2}{\alpha^2}\right)\cos(2\pi f_c t) \tag{2}$$

where α is the shape factor and $f_c=60.5$ GHz. The corresponding received signal is

$$r(t)=f(t)*h(t,\phi,\theta)+n(t) \tag{3}$$

where $n(t)$ is additive white Gaussian noise (AWGN) with zero mean and two sided power spectral density $N_0/2$, and $h(t,\phi,\theta)$ is the channel impulse response which can be expressed as

$$h(t,\phi,\theta)=\sum_{l=0}^{L}\sum_{k=0}^{K_l}\alpha_{k,l}\delta\left(t-T_l-\tau_{k,l}\right)\delta\left(\phi-\Omega_l-\omega_{k,l}\right)\delta\left(\theta-\Psi_l-\psi_{k,l}\right) \tag{4}$$

where $\delta(\cdot)$ is the Dirac delta function, L is the number of clusters, and K_l is the number of rays in the lth cluster. The scalars $\alpha_{k,l}$, $\tau_{k,l}$, $\omega_{k,l}$ and $\psi_{k,l}$ denote the complex amplitude, TOA, angle of arrival (AOA) and angle of departure (AOD) of the kth ray in the lth cluster, respectively. The average TOA, average AOA and average AOD of the l*th* cluster are denoted by T_l, Ω_l and Ψ_l, respectively. With directional antennas, (4) can be expressed as

$$h(t,\phi,\theta)=\beta\delta(t,\phi,\theta)+\sum_{l=0}^{L}\sum_{k=0}^{K_l}\alpha_{k,l}\delta\left(t-T_l-\tau_{k,l}\right)\delta\left(\phi-\Omega_l-\omega_{k,l}\right)\delta\left(\theta-\Psi_l-\psi_{k,l}\right) \tag{5}$$

where $\beta\delta(t,\phi,\theta)$ accounts for the LOS component which can be modeled as

$$\beta=20\log_{10}\left[\left(\frac{\mu_d}{d}\right)\left|\sqrt{G_{t1}G_{r1}}+\sqrt{G_{t2}G_{r2}}\Gamma_0\exp\left[j\frac{4\pi h_1 h_2}{\lambda d}\right]\right|\right]-PL_d\left(\mu_d\right)\ \text{dB} \tag{6}$$

$$PL_d\left(\mu_d\right)=20\log_{10}\left(\frac{4\pi d_0}{\lambda}\right)+A_{NLOS}+10n_d\log_{10}\left(\frac{d}{d_0}\right) \tag{7}$$

where PL_d, λ, A_{NLOS}, μ_d, Γ_0, h_1 and h_2 are the path loss of the first impulse response component, wavelength, NLOS attenuation, mean distance, reflection coefficient, and heights of the *TX* and *RX* antennas, respectively. G_{t1}, G_{t2}, G_{r1}, G_{r2} are the gains of the *TX* antenna for paths 1 and 2, and gains of the *RX* antenna for paths 1 and 2, respectively.

The received signal is first squared and the result integrated over a period T_b. The TOA estimate is then made by the decision device [14]. The duration of integration period is $3T_s/2$ to account for the inter-frame leakage due to the multipath signals [10]. The sample indices from the start of the integration period are $n\in(1,....,N_b)$, where $N_b=(3T_s)/(2T_b)$ is the number of samples. The integrator output is then given by

$$z[n]=\sum_{j=1}^{N_s}\int_{(j-1)T_s+(c_j+n-1)T_b}^{(j-1)T_s+(c_j+n)T_b}\left|r(t)\right|^2dt \tag{8}$$

where N_s is the number of pulses transmitted per data symbol. The mean and variance of z are $\mu_0=F\sigma^2$ and $\sigma_0^2=2F\sigma^4$ when the received signal is only noise, and $\mu_e=F\sigma^2+E_n$ and $\sigma_e^2=2F\sigma^4+4\sigma^2E_n$ when the received signal contains noise and the 60 GHz PPM signal, where E_n is the received energy for the nth block. The number of degrees of freedom is $F=2BT_b+1$ where B is the signal bandwidth [10]. In this paper, N_s is set to 1.

The TOA estimation is obtained by comparing the energy block values $z[n]$ with a threshold. The first value to exceed the threshold η is given by

$$\tau_{TC} = \left[\arg\min_{1 \le n \le N_b} \{ n \mid z[n] \ge \eta \} - 0.5 \right] T_b \tag{9}$$

It is difficult to determine the threshold directly from the received energy block values, so a normalized threshold is employed which is given by

$$\eta = \eta_{norm} \left[\max(z(n)) - \min(z(n)) \right] + \min(z(n)) \tag{10}$$

The problem is then how to obtain η_{norm}. There are two approaches to determining a suitable value, fitting an equation to the energy block values or using a fixing threshold (FT). Clearly using a FT is the simplest approach. In [9], η_{norm} was assumed to be an exponential function of the skewness for T_b = 1 ns and 4 ns. In [10], η_{norm} was considered to be a double exponential function of the kurtosis for T_b = 4 ns, and a linear function for T_b = 1 ns. A simple normalized threshold based on the ratio of the minimum to maximum values in an energy block was employed in [11]. However, none of these methods can provide good performance over a wide range of SNRs, which limits the TOA estimation accuracy. This is primarily due to the difficulty in identifying the arrival of the first signal component. In this paper, the mean absolute error (MAE) of the TOA estimates is used to evaluate an algorithm which can be expressed as

$$MAE = \frac{1}{N_t} \sum_{i=1}^{N_t} \left| t_i - t_i \right| \tag{11}$$

where t_i and t_i are the ith actual TOA and estimated TOA, respectively, and N_t is the number of TOA estimates.

3. Statistical Characteristics of the Signal Energy

In this section, the skewness, kurtosis and curl of the received energy block values are presented.

3.1 Skewness

The skewness of the received energy block values is given by

$$S = \frac{1}{\sigma^3 (N_b - 1)} \sum_{n=1}^{N_b} \left(z[n] - \bar{z} \right)^3 \tag{12}$$

where $\bar{z}$ and σ are the mean and standard deviation of the values, respectively. The skewness can be positive, negative, or even zero. When $S < 0$, the left tail is longer and the mass of the distribution is concentrated on the right. This distribution is said to be left-skewed, left-tailed, or skewed to the left. When $S > 0$, the right tail is longer and the mass of the distribution is concentrated on the left. This distribution is said to be right-skewed, right-tailed, or skewed to the right. When $S = 0$, the distribution is approximately Gaussian.

3.2 Kurtosis

The kurtosis of the received energy block values is given by

$$K = \frac{1}{\sigma^4 \left(N_b - 1\right)} \sum_{n=1}^{N_b} \left(z[n] - \bar{z}\right)^4 \tag{13}$$

where $\bar{z}$ and σ are the mean and standard deviation of the values, respectively. The kurtosis can be positive, negative, or even zero. When $K = 0$, the distribution is Gaussian. When $K < 0$, the distribution is sub-Gaussian, which means the tails are shorter than those of a Gaussian distribution. When $K > 0$, the distribution is super-Gaussian, which means the tails are longer than those of a Gaussian distribution. The kurtosis for a standard Gaussian distribution is three. For this reason, the kurtosis is often defined as K-3 (also denoted as excess kurtosis).

3.3 Curl

In vector calculus, the curl is an operator that describes the infinitesimal rotation of a vector field. It is usually defined with respect to a two or three dimensional vector. Here, the received values $z[n]$, $n \in \{1, 2, \cdots, N_b\}$, are considered to be an $N_b \times 1$ dimensional array denoted as **U**. The MATLAB function curl (**U**, **U**) [25] is employed to compute the curl, and the maximum is used to estimate the TOA. The curl will increase with increasing SNR.

3.4 Characteristics of the Statistical Parameters

For SNRs in the range 4 to 32 dB, 1000 impulse responses using the CM1.1 (residential LOS) and CM2.1 (residential NLOS) channel models from the IEEE 802.15.3c standard were obtained. A sampling rate of f_s = 9 GHz was employed. **Fig. 1** and **Fig. 2** present the kurtosis, skewness, and curl for an integration period of 4 ns. The frame duration is 200 ns and the chip duration is 1 ns. Every realization is uniformly distributed in the range 0 to T_s.

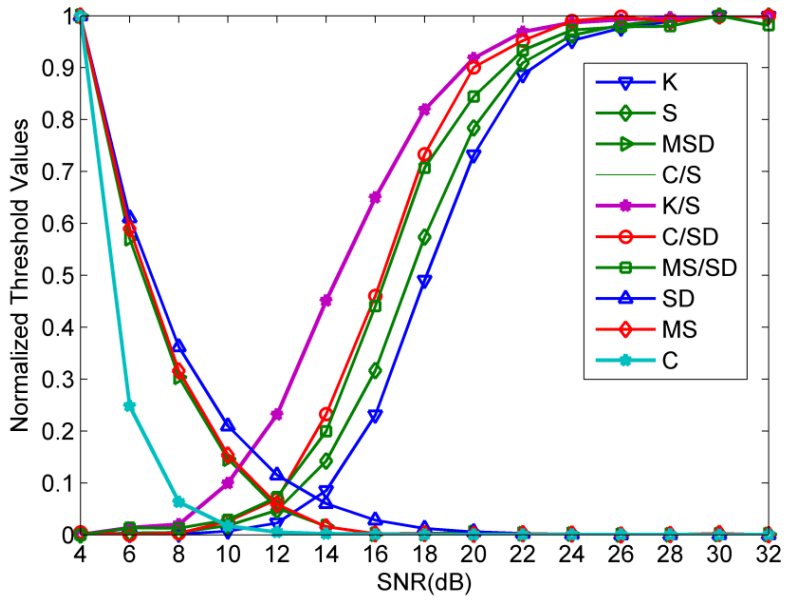

Fig. 1. The normalized statistical parameters with respect to SNR over channel CM1.1

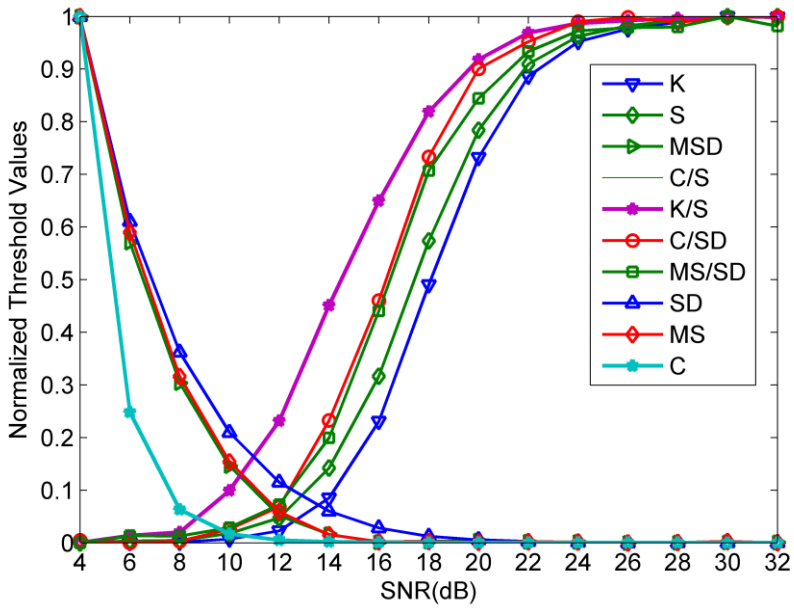

Fig. 2. The normalized statistical parameters with respect to SNR over channel CM2.1

These figures also show the standard deviation (SD), the maximum slope (MS), the product of maximum slope and standard deviation (MSD), the ratio of curl to skewness (C/S), the ratio of kurtosis to skewness (K/S), the ratio of curl to standard deviation (C/SD), and the ratio of maximum slope to standard deviation (MS/SD). These results indicate that the statistical parameters with respect to SNR are similar for the LOS and NLOS channels. The skewness, kurtosis, C/SD, K/S and MS/SD are all monotonically increasing functions of SNR, but K/S changes more quickly than the other parameters. Conversely, the maximum slope, standard deviation, curl and MSD are monotonically decreasing functions of SNR, but the curl decreases more quickly than the other parameters. Moreover, K/S increases slowly while the curl decreases quickly when SNR < 9 dB, while K/S increases quickly but the curl decreases slowly when SNR > 9 dB. These results show that no single parameter can be used to indicate the changes in SNR over a wide range of values.

4. Energy Detector based TOA Estimation using a Neural Network

In this section, a joint metric is proposed using the skewness, kurtosis and curl of the received energy block values. This metric provides a better indication of changes in the SNR than the statistical parameters considered in the previous section. A NN is used to determine the relationship between this metric and the threshold.

4.1 Joint Metric

The results in Section 3 show that no single statistical parameter can be used to indicate a wide range of SNR values. The MAE results presented in [9] were worse than those in [10] because the skewness can better reflect SNR variations than the kurtosis when SNR > 12 dB. Further, the MAE in [9] is larger than that in [12] when SNR < 12 dB. Consequently, none of these

techniques can provide good performance over a wide range of SNR values. To solve this problem, a joint metric using both *K*/*S* and C is employed which is given by

$$J = (K / S) \times 10 - C \times 2 \tag{14}$$

Table 1 shows that the standard deviation (SD) of the skewness, kurtosis and K/S increases with increasing SNR, but the former is less than the latter while the K/S values increase more rapidly. Conversely, the standard deviation of the curl and maximum slope decrease with increasing SNR, but the former is larger than the latter while the curl values decrease more rapidly. The rapid variations in the K/S and curl indicate that they are the best choices for a metric.

Table 1. The standard deviation of several statistical parameters

SNR (dB)	Kurtosis	Skewness	K/S	SD	Maximum Slope	Curl	MS/SD
4	0.82	0.30	19.5	0.35	7.05	49.0	32.3
6	0.83	0.30	20.7	0.27	5.43	15.8	34.4
8	0.87	0.31	22.2	0.22	4.37	7.08	34.1
10	1.01	0.32	23.8	0.19	3.71	3.29	37.2
12	1.36	0.37	25.8	0.16	3.16	2.19	43.1
14	2.05	0.45	28.1	0.14	2.77	1.35	60.4
16	3.03	0.55	30.8	0.12	2.48	0.94	69.5
18	3.90	0.61	34.2	0.11	2.27	0.82	76.2
20	4.45	0.63	38.4	0.10	2.11	0.95	76.8
22	4.82	0.64	43.7	0.092	1.98	0.74	93.7
24	5.11	0.63	50.8	0.086	1.89	0.68	88.2
26	5.35	0.63	57.8	0.080	1.80	0.68	94.0
28	5.55	0.62	59.2	0.075	1.73	0.63	101.5
30	5.73	0.62	64.6	0.071	1.66	0.51	99.1
32	5.88	0.62	66.0	0.068	1.61	0.68	100.6

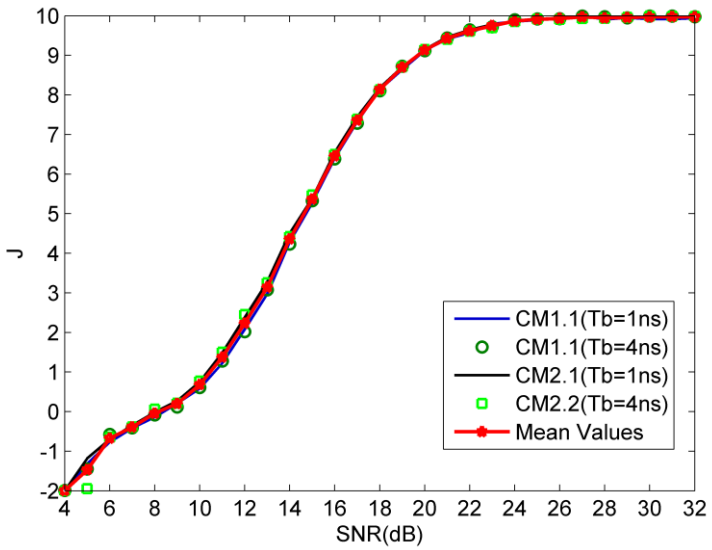

Fig. 3. Average value of *J* with respect to SNR

To confirm that J varies sufficiently over a wide range of SNRs, 1000 impulse responses were generated for each SNR in the range 4 to 32 dB using the channel models in the IEEE 802.15.3c standard. The mean values of J are given in **Fig. 3**. These results show that J is a monotonically increasing function over the entire range of SNR values. Further, J is independent of the integration period and channel.

4.2 Threshold Determination

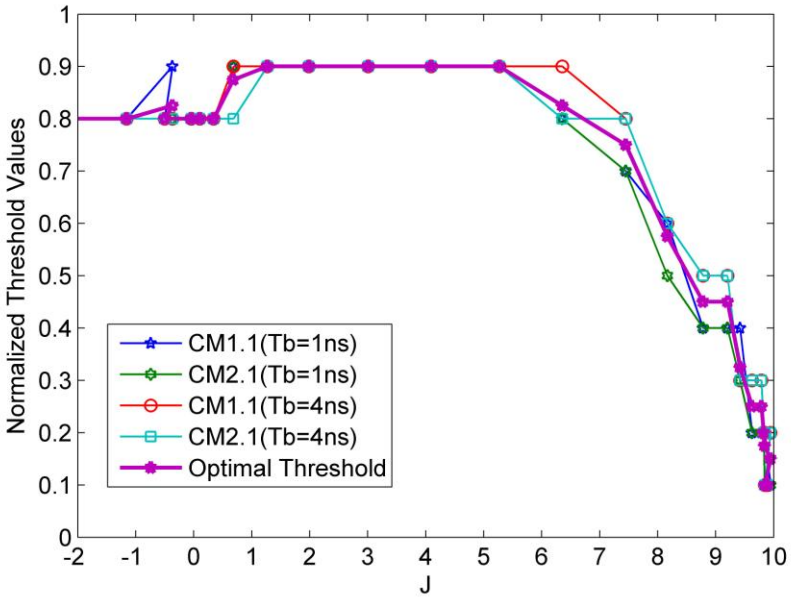

Fig. 4. The normalized threshold versus J

In this section, the NN based threshold selection algorithm for TOA estimation is developed for the 60 GHz MMW system. The values of J are rounded to the integer or half integer. To find the best normalized threshold η_{best} using J, the relationship of both the MAE and η_{norm} with respect to J, the channel and the integration period is examined. The results obtained indicate that the MAE decreases with increasing J and the minimum MAE is lower with increasing J [10]. Therefore, η_{norm} with regard to the minimum MAE is referred to as η_{best}. These best normalized thresholds are shown in **Fig. 4**. The results obtained indicate that J and η_{best} are independent of the integration period and channel. Consequently, the average η_{best}, denoted as the optimal threshold, is given by

$$\eta_{opt}(J) = \text{mean} \sum \eta_{opt}^{(T_b = i\,ns)}(J) \tag{15}$$

where

$$\eta_{opt}^{T_b = i\,ns}(J) = \text{mean}\left[\eta_{best}^{(CM1.1,\,T_b = i\,ns)}(J) + \eta_{best}^{(CM2.1,\,T_b = i\,ns)}(J)\right] \tag{16}$$

and i is the integration period in ns. To evaluate the performance of the proposed threshold selection algorithm, it is compared with several well-known ED based TOA algorithms. The

integration periods considered are 1 ns and 4 ns, so the optimal threshold value is set to

$$\eta_{opt}(J) = \text{mean}\left[\eta_{opt}^{(T_b=1ns)}(J) + \eta_{opt}^{(T_b=4ns)}(J)\right] \tag{17}$$

where

$$\eta_{opt}^{T_b=ins}(J) = \text{mean}\left[\eta_{best}^{(\text{CM1.1},\,T_b=ins)}(J) + \eta_{best}^{(\text{CM2.1},T_b=ins)}(J)\right] \tag{18}$$

4.3 NN Based TOA Estimation Algorithm

In this paper, a BPNN is employed which has three layers, an input layer, a hidden layer and an output layer. The parameters of the feedforward network in each layer are independent, so they must be tuned, which can make the computational complexity of the NN high. The number of neurons in the hidden layer has a significant effect on the NN performance [26].

To ensure the stability and convergence of the NN, the algorithm was examined to initialize the weights and biases in different layers via simulation as in [27]. The number of neurons was determined based on the mean squared error (MSE) averaged over different sets of training data. The number of neurons considered was 2 to 40, and the NN was trained 200 times for each value and the average MSE obtained. The number of times the MSE is less than $1e^{-10}$ increases as the number of neurons increases, but the computational complexity also increases. With 16 neurons, more than 90% of the MSEs are less than $1e^{-10}$, and this percentage increases minimally as the number of neurons is increased. Thus, 16 neurons are used in the hidden layer of the NN for TOA estimation.

As the η_{norm} ranges from 0 to 1, the log sigmoid function is used as the transfer function between layers. The well-known Levenberg-Marquardt (LM) algorithm is used to train the NN, so the weights and biases in the layers are updated based on the LM optimization in [28]. The LM algorithm is typically one of the fastest for BPNN training. The NN has one input and one output, and only 26 sets of $\eta_{opt} - J$ (J = -2 to 10 for T_b = 1 ns and 4 ns), are employed, so the memory requirements are moderate. To confirm the relationship between J and η_{opt}, the integer values of J for T_b = 1 ns and 4 ns were used to train the NN. To obtain the NN with the best performance, 100 iterations were performed for each integration period, and the NN with the lowest MSE was selected.

4.4 Validation of the Trained NN

Table 2. Neural network validation results

Validation	T_b (ns)	NN input (J)	MSE ($\times e^{-33}$)
Internal	1	[-2, -1,…,10]	9.90
External	1	[-1.5, …, 9.5]	6.16
Internal	4	[-2, -1, …, 10]	9.90
External	4	[-1.5, …, 9.5]	6.16

To evaluating the effectiveness of the NN, two validations were performed, internal validation with integer values of J in the range -2 to 10, and external validation with half integer values of J in the range -1.5 to 9.5. The corresponding results are given in **Fig. 5** and **Fig. 6**, and show that the output of the trained NN agree well with η_{opt} for both integration periods. Thus, the

NN parameters can be determined based on an estimation of the channel statistics. Consequently, the proposed NN can be employed in any channel environment so long as the NN parameters are adjusted appropriately. **Table 2** shows that the MSE of the internal validation is $9.9e^{-33}$ while the MSE of the external validation is $6.16e^{-33}$, which are excellent results.

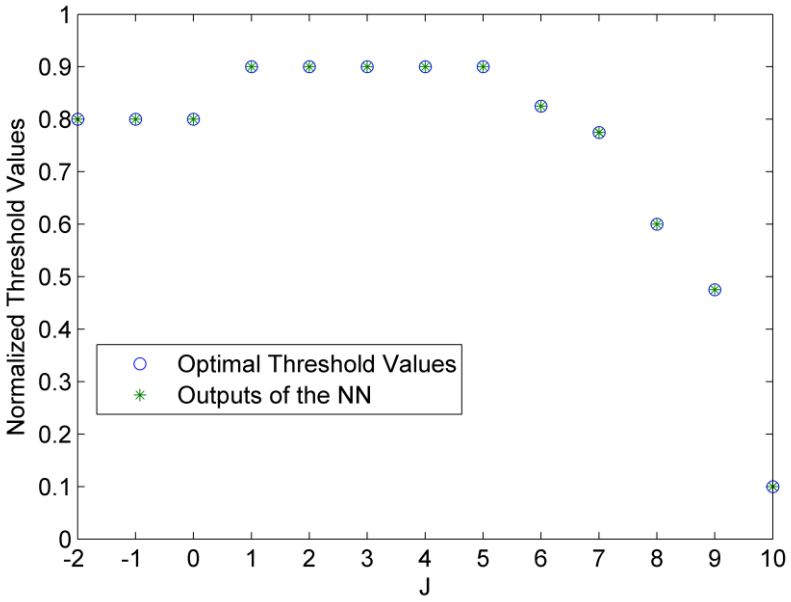

Fig. 5. Internal validation results for the proposed NN

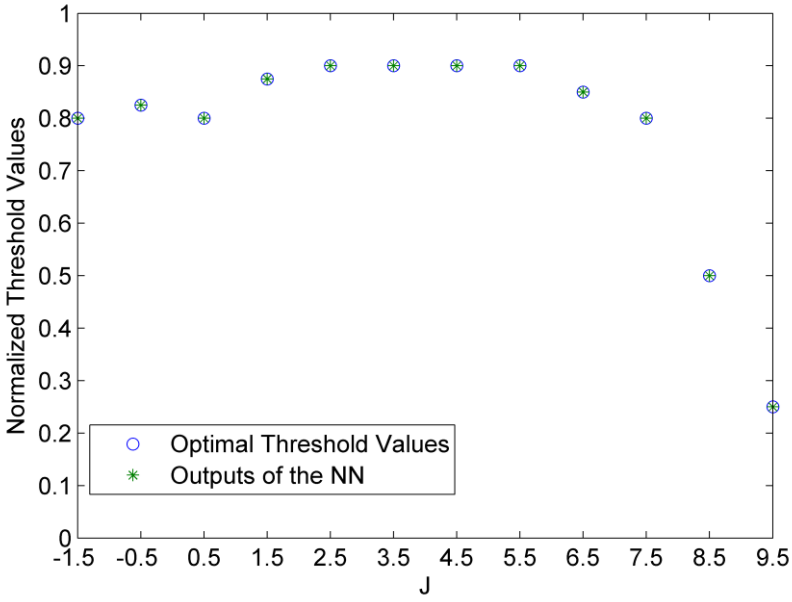

Fig. 6. External validation results for the proposed NN

5. Results and Discussion

In this section, the MAE of the proposed NN based algorithm is compared with that of other ED threshold algorithms. The 60 GHz residential LOS and NLOS channel models from the IEEE 802.15.3c standard are employed, and the results are averaged over 1000 channel realizations. The system parameters are the same as used previously.

Fig. 7 and **Fig. 8** show the MAE of the proposed NN based algorithm for SNR values in the range -4 to 30 dB for the CM1.1 and CM2.1 channel models, respectively, with different integration periods. These results show that this algorithm provides better performance than the other ED TOA algorithms over a wide range of SNRs. The MAE in the residential LOS channel is less than that in the residential NLOS channel by as much as 20 ns. In the majority of cases, the MAE for $T_b = 1$ ns is less than that for $T_b = 4$ ns by up to 1.2 ns with either channel model. As a consequence, the integration period is a significant factor which affects TOA accuracy. In particular, the MAE increases as the integration period is increased. Fortunately, the NN based TOA estimation algorithm is independent of the integration period, which resolves this problem.

Table 3 shows the average MAE for six TOA estimation algorithms. Where NN is the proposed neural network based algorithm, MES is the maximum energy selection algorithm, K is the kurtosis based algorithm, S is the skewness based algorithm, MMR is the ratio of maximum to minimum energy based algorithm, and FT is the fixed threshold algorithm with normalized thresholds 0.4 and 0.6. The proposed NN based algorithm provides the lowest average MAE in all cases.

Fig. 7 and **Fig. 8** show that the NN based algorithm provides the best overall performance, particularly at low SNRs. When the SNR is high, the performance difference becomes quite small. In particular, the MAE of the NN based algorithm is 0.1 ns less than that of the skewness based algorithm when SNR = 24 dB. In the majority of cases, our NN based algorithm provides the best performance. Further, the other algorithms have poor performance when SNR < 10 dB.

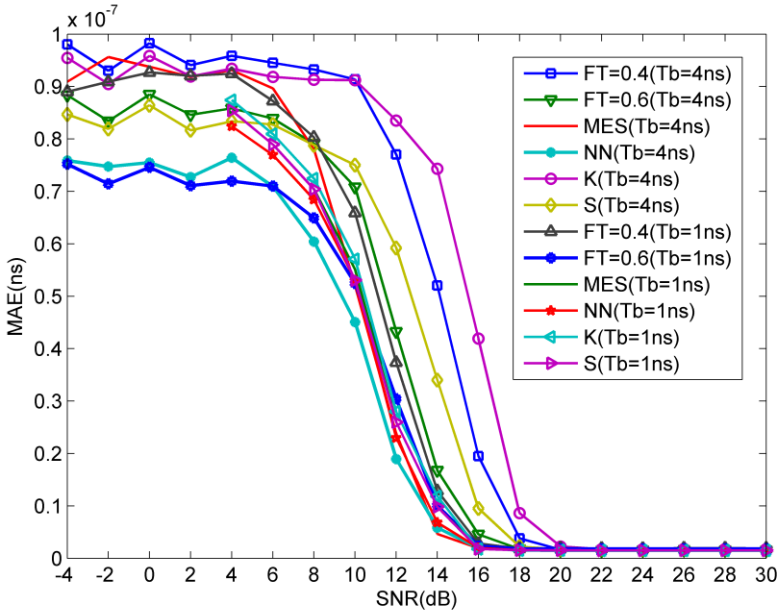

Fig. 7. MAE versus SNR for different TOA algorithms with channel CM1.1

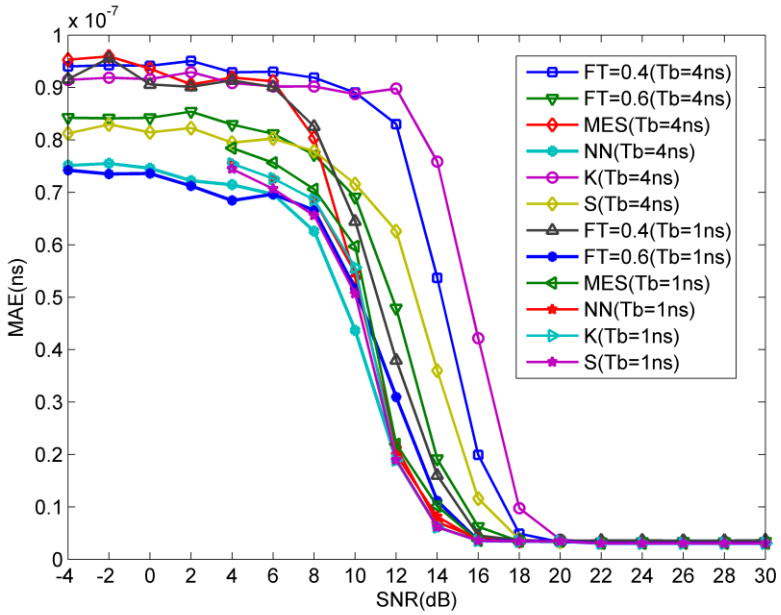

Fig. 8. MAE versus SNR for different TOA estimation algorithms with channel CM2.1

Table 3. Average MAE (ns) for several TOA estimation algorithms

Channel	T_b	NN	K	MES	MMR	FT0.4	FT0.6	S
CM1.1	1ns	30.729	39.626	40.398	46.264	51.114	41.116	35.626
	4ns	33.789	41.779	42.045	48.880	53.384	42.796	38.779
CM2.1	1ns	32.093	41.288	41.644	47.313	51.404	41.385	39.288
	4ns	34.353	44.517	43.341	49.947	53.663	42.868	42.517

6. Conclusions

A threshold selection algorithm for TOA estimation based on a NN was presented which employs 60 GHz MMW signals. This algorithm is based on an energy detector (ED) which has low complexity. A joint metric was proposed based on the skewness, kurtosis and curl of the received energy block values. The best thresholds were obtained for the residential LOS (CM1.1) and NLOS (CM2.1) channel models from the IEEE 802.15.3c standard with different integration periods. The proposed algorithm was shown to provide better TOA estimates compared to other ED based algorithms in the majority of cases. This is because the NN based algorithm adapts better to changes in the SNR, and is independent of the integration period and channel model.

References

[1] Z. Lei, Z. Chunyuan, W. Hongrui, W. Yan, Q. He and Y. Zhiping, "A fully integrated 60 GHz five channel CMOS receiver with 7GHz ultra-wide band width for IEEE 802.11ad standard," *China Communications*, vol. 11, no. 6, pp. 42-50, June, 2014. Article (CrossRef Link).

[2] N. R. Leonor, R. F. S. Caldeirinha, T. R. Fernandes and M. García Sánchez, "A Simple Model for Average Reradiation Patterns of Single Trees Based on Weighted Regression at 60 GHz," *IEEE Transactions on Antennas and Propagation*, vol. 63, no. 11, pp. 5113-5118, November, 2015. Article (CrossRef Link).

[3] Takuya Sakamoto, Shigeaki Okumura, Ryosuke Imanishi, Hirofumi Taki, Toru Sato, Mototaka Yoshioka, Kenichi Inoue, Takeshi Fukuda and Hiroyuki Sakai, "Remote heartbeat monitoring from human soles using 60-GHz ultra-wideband radar," *IEICE Electronics Express*, vol. 12, no. 21, pp. 20150786, October, 2015. Article (CrossRef Link).
[4] Jian Song and Kwan-Wu Chin, "A survey of single and multi-hop link schedulers for mmWave wireless systems," *Ad Hoc Networks*, vol. 33, pp. 269-283, October, 2015.Article (CrossRef Link).
[5] X. Ge, B. Yang, J. Ye, G. Mao, C. X. Wang and T. Han, "Spatial Spectrum and Energy Efficiency of Random Cellular Networks," *IEEE Transactions on Communications*, vol. 63, no. 3, pp. 1019-1030, March, 2015. Article (CrossRef Link).
[6] X. Ge, H. Cheng, M. Guizani and T. Han, "5G wireless backhaul networks: challenges and research advances," *IEEE Network*, vol. 28, no. 6, pp. 6-11, November, 2014. Article (CrossRef Link).
[7] N. Chahat, G. Valerio, M. Zhadobov and R. Sauleau, "On-Body Propagation at 60 GHz," *IEEE Transactions on Antennas and Propagation*, vol. 61, no. 4, pp. 1876-1888, April, 2013. Article (CrossRef Link).
[8] Yi Zhu, Chong Tang, Lixing Song, Shaoen Wu and Saâd Biaz, "Analytical and comparative investigation of 60 GHz wireless channels," *Telecommunication Systems*, vol. 60, no. 1, pp. 179-186, September, 2015. Article (CrossRef Link).
[9] Hao Zhang, Xue-rong Cui and T. Aaron Gulliver, "Threshold Selection for Ultra-Wideband TOA Estimation Based on Skewness Analysis," *Lecture Notes in Computer Science*, vol. 6905, pp. 503-513, September, 2011. Article (CrossRef Link).
[10] I. Guvenc and Z. Sahinoglu, "Threshold selection for UWB TOA estimation based on kurtosis analysis," *IEEE Communications Letters*, vol. 9, no. 12, pp. 1025-1027, December, 2005. Article (CrossRef Link).
[11] Guvenc, Ismail and Sahinoglu, Zafer, "Threshold-based TOA estimation for impulse radio UWB systems," in *Proc. of 2005 IEEE Int. Conf. on Ultra-Wideband*, pp. 420-425, September 5-8, 2005. Article (CrossRef Link).
[12] Hao Zhang, Xue-rong Cui and T Aaron Gulliver, "Remotely-sensed TOA interpretation of synthetic UWB based on neural networks," *Eurasip Journal on Advances in Signal Processing*, vol. 2012, August, 2012. Article (CrossRef Link).
[13] Ahmadreza Jafari, Luca Petrillo, Julien Sarrazin, David Lautru, Philippe De Doncker and Aziz Benlarbi-Delai, "TDOA estimation method using 60 GHz OFDM spectrum," *International Journal of Microwave and Wireless Technologies*, vol. 7, no. 1, pp. 31-35, September, 2014. Article (CrossRef Link).
[14] Ranjay Hazra and Anshul Tyagi, "A Survey on Various Coherent and Non-coherent IR-UWB Receivers," *Wireless Personal Communications*, vol. 79, no. 3, pp. 2339-2369, December, 2014. Article (CrossRef Link).
[15] Muhammad Asif Zahoor Raja, Fiaz Hussain Shah, Abdul Ahad Khan and Najeeb Alam Khan, "Design of bio-inspired computational intelligence technique for solving steady thin film flow of Johnson-Segalman fluid on vertical cylinder for drainage problems," *Journal of the Taiwan Institute of Chemical Engineers*, vol. 60, pp. 59-75, March, 2016. Article (CrossRef Link).
[16] M. G. Di Benedetto and B. R. Vojcic, "Ultra-wide band wireless communications: A tutorial," *Journal of Communications and Networks*, vol. 5, no. 4, pp. 290–302, December 2003. Article (CrossRef Link).
[17] S. Niranjayan and N.C. Beaulieu, "Novel Adaptive Nonlinear Receivers for UWB Multiple Access Communications," *IEEE Transactions on Wireless Communications*, vol. 12, no. 5, pp. 2014–2023, October, 2013. Article (CrossRef Link).
[18] Pengxiao Li, Hongwei Chen, Minghua Chen and Shizhong Xie, "Beyond 2.5Gb/s Photonic Generation and Wireless Transmission of Different Pulse Modulation Formats for a High Speed Impulse Radio UWB over Fiber System," in *Proc. of Optical Fiber Communication Conference 2011*, March 6-10, 2011. Article (CrossRef Link).

[19] H. Xiong, W. Zhang, Z. Du, B. He and D. Yuan, "Front-End Narrowband Interference Mitigation for DS-UWB Receiver," *IEEE Transactions on Wireless Communications*, vol. 12, no. 9, pp. 4328–4337, September, 2013. Article (CrossRef Link).
[20] P. Kalansuriya, N.C. Karmakar and E. Viterbo, "On the Detection of Frequency-Spectra-Based Chipless RFID Using UWB Impulsed Interrogation," *IEEE Transactions on Microwave Theory Technology*, vol. 60, no. 12, pp. 4187–4197, December, 2012. Article (CrossRef Link).
[21] X. R. Lee, C. L. Chen, H. C. Chang and C. Y. Lee, "A 7.92 Gb/s 437.2 mW Stochastic LDPC Decoder Chip for IEEE 802.15.3c Applications," *IEEE Transactions on Circuits and Systems I: Regular Papers*, vol. 62, no. 2, pp. 507-516, February, 2015. Article (CrossRef Link).
[22] W. C. Liu, T. C. Wei, Y. S. Huang, C. D. Chan and S. J. Jou, "All-Digital Synchronization for SC/OFDM Mode of IEEE 802.15.3c and IEEE 802.11ad," *IEEE Transactions on Circuits and Systems I: Regular Papers*, vol. 62, no. 2, pp. 545-553, February, 2015. Article (CrossRef Link).
[23] J. Kim, A. Mohaisen and J. K. Kim, "Fast and Low-Power Link Setup for IEEE 802.15.3c Multi-Gigabit/s Wireless Sensor Networks," *IEEE Communications Letters*, vol. 18, no. 3, pp. 455-458, March, 2014. Article (CrossRef Link).
[24] H. Zhang, T. t. Lu and T. A. Gulliver, "Pulse waveforms for 60 GHz M-ary pulse position modulation communication systems," *IET Communications*, vol. 7, no. 2, pp.169-179, January, 2013. Article (CrossRef Link).
[25] César Pérez López, MATLAB Matrix Algebra, Apress, Berlin, 2014. Article (CrossRef Link).
[26] Francesco Camastra and Alessandro Vinciarelli, *Machine Learning for Audio, Image and Video Analysis: Theory and Applications*, 2nd Edition, Springer, Berlin, 2015. Article (CrossRef Link).
[27] R. Vicen-Bueno, R. Carrasco-Á lvarez, M. Rosa-Zurera, J. C. Nieto-Borge and M. P. Jarabo-Amores, "Artificial Neural Network-Based Clutter Reduction Systems for Ship Size Estimation in Maritime Radars," *Eurasip Journal on Advances in Signal Processing*, vol. 2010, March, 2010. Article (CrossRef Link).
[28] G. Lera and M. Pinzolas, "Neighborhood based Levenberg-Marquardt algorithm for neural network training," *IEEE Transactions on Neural Networks*, vol. 13, no. 5, pp. 1200-1203, September, 2002. Article (CrossRef Link).

Xiaolin Liang is a doctoral candidate in College of Information Science and Engineering, Ocean University of China. His research interests include ultra-wideband radio systems and 60 GHz wireless communication system.

Hao Zhang was born in Jiangsu, China, in 1975. He received his B.S. degree in telecom engineering and industrial management from Shanghai Jiaotong University, China, in 1994, his MBA degree from New York Institute of Technology, USA, in 2001, and his Ph.D. degree in electrical and computer engineering from the University of Victoria, Canada, in 2004. His research interests include ultra-wideband radio systems, MIMO wireless systems, and spectrum communications. From 1994 to 1997, he was the Assistant President of ICO (China) Global Communications Company. He is now a Professor of the Department of Electrical Engineering at Ocean University of China. He also holds an adjunct Assistant Professor at university of Victoria. He is an IEEE Senior Member.

T. Aaron Gulliver received the Ph.D. degree in electrical and computer engineering from the University of Victoria, Victoria, British Columbia, Canada, in 1989. From 1989 to 1991, he was employed as a Defence Scientist at the Defence Research Establishment Ottawa, Ottawa, Ontario, Canada. He has held academic positions at Carleton University, Ottawa, and the University of Canterbury, Christchurch, New Zealand. He joined the University of Victoria in 1999 and is a Professor in the Department of Electrical and Computer Engineering. He is a Senior Member of the IEEE and a Member of the Association of Professional Engineers of Ontario, Canada. In 2002, he became a Fellow of the Engineering Institute of Canada. His research interests include information theory and communication theory, algebraic coding theory, cryptography, construction of optimal codes, turbo codes, spread-spectrum communications, space-time coding, and ultra-wideband communications.